Different subregions of monkey lateral prefrontal cortex respond to abstract sequences and their components

Authors: Nadira Yusif Rodriguez[1], Aarit Ahuja[1], Debaleena Basu[1,2], Theresa H. McKim[3], and Theresa M. Desrochers*[1,4,5]

Affiliations:

1. Department of Neuroscience, Brown University
2. Department of Biosciences and Bioengineering, IIT Bombay, Mumbai, Maharashtra, India
3. Department of Biology & Institute for Neuroscience, University of Nevada, Reno
4. Department of Psychiatry and Human Behavior, Brown University
5. Robert J. and Nancy D. Carney Institute for Brain Sciences, Brown University

*Corresponding Author: Theresa M. Desrochers, theresa_desrochers@brown.edu

Abbreviated title: Monkey LPFC regions respond to sequence components

Conflict of Interest Statement: The authors declare no competing financial interests.

Acknowledgements

This study was supported by the National Science Foundation (NSF) Established Program to Stimulate Competitive Research (EPSCoR) Neural Basis of Attention Grant 1632738 (N.Y.R.

and T.M.D.), the National Institute of General Medical Sciences (NIGMS)-National Institutes of Health (NIH) Initiative to Maximize Student Development Grant IMSD R25GM083270 (N.Y.R.), the NIH-NIGMS Grant COBRE P20GM103645 (T.M.D), NIH National Institutes of Mental Health (NIMH) R21MH125010 (T.M.D.), NSF Faculty Early Career Development (CAREER) Program Award BCS-2143656 (T.M.D.), NIMH Research Project Grant R01MH131615 (T.M.D.), and the Carney Institute for Brain Science Innovation Award (T.M.D.). Part of this research was conducted using computational resources and services at the Center for Computation and Visualization, Brown University (NIH Grant S10OD025181).

N.Y.R.'s present address: Massachusetts General Hospital, Athinoula A. Martinos Center for Biomedical Imaging, Charlestown, MA.

We thank Matthew Maestri for his assistance with animal training and data collection. We thank Dr. Michael Worden, Lynn Fanella, Fabienne McEleney, and Brown University's MRI Facilities staff for their support and guidance throughout this project. We thank Dr. Lucija Jankovic-Rapan, Dr. Nicola Palomero-Gallagher and Dr. Seán Froudist-Walsh for their assistance and sharing of the MEBRAINS atlas and regions of interest used for analysis. We also thank Dr. David Sheinberg, Dr. Amitai Shenhav, Dr. Katherine Conen, and Hannah Doyle for their continued support throughout this project and preparation of this publication as well as members of both the Sheinberg and the Desrochers Labs for many helpful discussions and contributions.

Author Contributions

Nadira Yusif Rodriguez: Conceptualization, Investigation, Formal analysis, Writing - Original Draft, Writing - Review & Editing, Visualization. Aarit Ahuja: Investigation, Writing - Review & Editing. Debaleena Basu: Conceptualization, Investigation, Writing - Review & Editing. Theresa H. McKim: Conceptualization, Investigation, Writing - Review & Editing. Theresa M. Desrochers: Conceptualization, Methodology, Investigation, Writing - Original Draft, Writing - Review & Editing, Supervision, Resources, Funding acquisition.

Abstract

Sequential information permeates daily activities, such as when watching for the correct series of buildings to determine when to get off the bus or train. These sequences include periodicity (the spacing of the buildings), the identity of the stimuli (the kind of house), and higher-order more abstract rules that may not depend on the exact stimulus (e.g. house, house, house, business). Previously, we found that the posterior fundus of area 46 in the monkey lateral prefrontal cortex (LPFC) responds to rule changes in such abstract visual sequences. However, it is unknown if this region responds to other components of the sequence, i.e., image periodicity and identity, in isolation. Further, it is unknown if this region dissociates from other, more ventral LPFC subregions that have been associated with sequences and their components. To address these questions, we used awake functional magnetic resonance imaging in three male macaque monkeys during two no-report visual tasks. One task contained abstract visual sequences, and the other contained no visual sequences but maintained the same image periodicity and identities.

We found the fundus of area 46 responded only to abstract sequence rule violations. In contrast, the ventral bank of area 46 responded to changes in image periodicity and identity, but not changes in the abstract sequence. These results suggest a functional specialization within anatomical substructures of LPFC to signal different kinds of stimulus regularities. This specialization may provide key scaffolding to identify abstract patterns and construct complex models of the world for daily living.

Significance Statement

Daily tasks, such as a bus commute, require tracking or monitoring your place (same, same, same, different building) until your stop. Sequence components such as rule, periodicity (timing), and item identity are involved in this process. While prior work located responses to sequence rule changes to area 46 of monkey lateral prefrontal cortex (LPFC) using awake monkey fMRI, less was known about other components. We found that LPFC subregions differentiated between sequence components. Area 46 posterior fundus responded to abstract visual sequence rule changes, but not to changes in image periodicity or identity. The converse was true for the more ventral, adjacent shoulder region. These results suggest that interactions between adjacent LPFC subregions provide key scaffolding for complex daily behaviors.

Introduction

When commuting to work, such as when taking a bus, you may internally track house, house, house, store (same, same, same, different building) until you arrive at your stop. This recognition illustrates an essential process: the monitoring of abstract sequences. These sequences are abstract because they do not depend on the identity of the individual stimuli (e.g., changing the color of the house). The same system that facilitates sequential tracking also enables the detection of changes or deviations to an existing sequence. Sequences are defined by multiple elements that we specifically refer to as components. These sequential components include item identity, periodicity (temporal structure), and rule. Abstract sequence rule deviations may encompass changes in these individual sequence components. How does the brain track changes to sequences and their components?

We identified a brain region that responds to abstract sequence deviations, but whether the same or other regions also monitor changes in sequential components has not been tested. Previously, we identified a specific subregion within the fundus of posterior area 46 of the lateral prefrontal cortex (LPFC) as uniquely responding to sequential changes using awake monkey functional magnetic resonance imaging (fMRI) (Yusif Rodriguez et al., 2023). Beyond the rule that these abstract sequences followed, they had two (previously mentioned) main components: image identity and periodicity. These components were controlled for when determining responses to infrequent changes in the abstract visual sequence. However, LPFC is also known to respond to changes in image identity or periodicity. Responses to infrequent (sometimes referred to as “oddball”) stimuli have been reported in monkey LPFC using an array of techniques (Chao et al., 2018; Camalier et al., 2019; Grohn et al., 2020). Changes in stimulus periodicity could also elicit responses in LPFC because responses in LPFC are modulated by the duration preceding the

111 auditory or visual stimulus (Onoe et al., 2001; Genovesio et al., 2006; Chiba et al., 2021).
112 Therefore, the question arises as to whether the same, abstract sequence coding, or other LPFC
113 subregions respond to changes in image periodicity or identity alone.

114 The ventral LPFC (VLPFC) is a prime candidate as another subregion within the LPFC
115 that could respond to sequential components. FMRI studies in macaques have shown VLPFC
116 activity during auditory sequential tasks and sequence deviants (Wang et al., 2015; Vergnieux
117 and Vogels, 2020). Studies using electrophysiology provided evidence for the representation of
118 generalizable sequential structures and changes to these structures in neuronal population
119 responses within VLPFC (Esmailpour et al., 2023; Bellet et al., 2024). VLPFC also responds to
120 non-sequential information that shares similar features with sequential tasks, such as prediction
121 error (Uhrig et al., 2014; Chao et al., 2018) and responses to infrequent ("oddball") items (Uhrig
122 et al., 2014; Suda et al., 2022). VLPFC is often observed as more directly representing sensory
123 visual information (compared to DLPFC, which can be more spatial or action oriented).
124 Responses in VLPFC for non-spatial object-based features include color, shape, and object type
125 (Meyer et al., 2011; Yamagata et al., 2012; Tang et al., 2021; Xu et al., 2022). Thus, there is
126 evidence to suggest that VLPFC could respond to sequential components and abstract sequences,
127 underscoring the importance for dissociating between LPFC subregions.

128 To dissociate between LPFC subregions, we defined a more ventral, yet adjacent brain
129 area. Historically, many conventions have been applied to naming subregions within the LPFC
130 (Walker, 1940; Petrides and Pandya, 1999; Rapan et al., 2023). While some studies refer to
131 VLPFC as the region ventral to the arcuate sulcus, primarily Brodmann area 44 and potentially
132 parts of 6VR (Rapan et al., 2023), others refer to the region ventral to the principal sulcus and
133 dorsal to the arcuate sulcus that can include Brodmann areas 46, 9/46, 45A, and 45B along with

134 more anterior territory such as Brodmann areas 47 and 12 (Rapan et al., 2023). Our purpose here
135 is not to adjudicate among the definitions, but take advantage of a commonality that, in general,
136 more ventral regions of the LPFC are more biased towards sensory, object-based, or non-spatial
137 information (Meyer et al., 2011; Yamagata et al., 2012; Tang et al., 2021; Xu et al., 2022).
138 Therefore, an area that is more ventral, yet adjacent to the subregion in area 46 where we
139 previously observed sequential responses is an ideal candidate for comparison. A region defined
140 as thus would not make assumptions about naming conventions and still be clearly within the
141 LPFC. Using this region, we determined if there were differences in abstract sequence or
142 component representation between the two LPFC sub-regions.

143 To address the questions of whether LPFC subregions dissociate based on 1) responses to
144 abstract sequences, and 2) responses to sequence components (image identity and periodicity),
145 we conducted an awake monkey fMRI experiment. Monkeys performed two no-report tasks, one
146 that contained abstract visual sequences (previously reported on in (Yusif Rodriguez et al.,
147 2023)), and another that did not contain abstract visual sequences but maintained the image
148 identities and timing structure of the sequence task. We defined two LPFC subregions using a
149 parcellation of the PFC (Rapan et al., 2023): the posterior fundus of area 46 (p46f) that
150 overlapped with the previously identified sequence responsive subregion (Yusif Rodriguez et al.,
151 2023), and the adjacent posterior ventral shoulder of area 46 (p46v). Building on our previous
152 observations, we hypothesized that p46f would show responses unique to changes in abstract
153 visual sequences and not to their image identity and periodicity components. We hypothesized
154 the contrary for p46v: responses to changes in sequence components but not sequences
155 themselves. Our results broadly supported these hypotheses, with sequence responses in p46f and
156 not p46v, and responses to image identity and periodicity in p46v. These results further our

157 understanding of the representation of abstract visual sequences in adjacent subregions in the
158 LPFC.
159
160

161 **Methods**

162 **Participants**

163 We tested three adult male rhesus macaques (ages spanning 6-12 years during data collection, 9-
164 14 kg). All procedures followed the NIH Guide for Care and Use of Laboratory Animals and
165 were approved by the Institutional Animal Care and Use Committee (IACUC) at Brown
166 University.

167 **Task Design and Procedure**

168 All visual stimuli used in this study were displayed using an OpenGL-based software system
169 developed by Dr. David Sheinberg at Brown University. The experimental task was controlled
170 by a QNX real-time operating system using a state machine. Eye position was monitored using
171 video eye tracking (Eyelink 1000, SR Research). Stimuli were displayed at the scanner on a 24-
172 inch BOLDscreen flat-panel display (Cambridge Systems).
173

174 Each image presentation consisted of fractal stimulus (approximately 8° visual angle) with
175 varying colors and features. Fractals were generated using MATLAB for each scanning session
176 using custom scripts based on stimuli from (Kim and Hikosaka, 2013) following the instructions
177 outlined in (Miyashita et al., 1991). For each scan session, new, luminance matched fractal sets
178 were generated. All stimuli were presented on a gray background, with a fixation spot that was

always present on the screen superimposed on the images. To provide behavioral feedback, the fixation spot was yellow when the monkey was successfully maintaining fixation and red if the monkey was not fixating. Stimuli were displayed for 0.1, 0.2, or 0.3 s each, depending on the task, sequence type, and timing template.

The timing of liquid rewards was the same across tasks and not contingent on image presentations, only on the monkey maintaining fixation. Rewards were delivered on a graduated schedule such that the longer the monkey maintained fixation, the more frequent rewards were administered (Leite et al., 2002). The first reward was given after 4 s of continuous fixation. After two consecutive rewards of the same fixation duration, the fixation duration required to obtain reward was decreased by 0.5 s. The minimum duration between rewards that the monkey could obtain was 0.5 s. Fixation had to be maintained within a small window (typically 3° of visual angle) around the fixation spot to not break fixation. The only exception was a brief time window (0.32 s) provided for blinks. If the monkey's eyes left the fixation window and returned within that time window, it would not trigger a fixation break. If fixation was broken, the reward schedule would restart at the maximum 4 s duration required to obtain reward.

Tasks were organized into runs. Runs typically lasted approximately 10 min and only one task was shown for each run. The order of tasks was pseudo-randomized within a scanning session (one day) to balance the overall number of runs for each task and their presentation order. Monkeys completed approximately 10 runs in a session.

Runs were initiated according to the monkey's fixation behavior to ensure that the monkey was not moving and engaged in the task before acquiring functional images. During this pre-scan period, a fixation spot was presented. Once the monkey successfully acquired this fixation spot and received approximately four liquid rewards (12 – 16 s), functional image acquisition and the first habituation block were initiated. Monkeys maintained fixation for the duration of the run.

<u>Abstract Sequence Viewing (SEQ) Task</u>

The details of the abstract sequence viewing task have been previously described (Yusif Rodriguez et al., 2023) and are briefly summarized here. There were a total of five sequence types and nine timing templates (**Figure 1**). The inter-sequence interval was jittered to decorrelate across timing templates (mean 2 s, 0.25-8 s).

Habituation Sequences

Habituation sequences used images drawn from a pool of four fractals [A, B, C, D] and were arranged to follow one of two possible rules: three the same, one different, and four the same. All four-image sequences used one of six possible timing templates (**Figure 1C**).

Deviant Sequences

Deviant sequences used images drawn from a different pool of three fractals [E, F, G]. All deviant images were displayed for 0.2 s and used the same general timing template (adjusted for the number of items in the sequence). There were four deviant types, as follows:

- *New Items, Same Rule (NISR)*: four-image sequences that follow the same rule as the habituation sequences.
- *Rule Deviants*: four-image sequences that follow the alternate rule not used in the habituation sequences.

- *Number Deviants*: two- or six-image sequences that follow the same rule as the habituation sequences.
- *Double Deviants*: combine the rule and number deviant types and contain two- or six-image sequences that follow the alternate rule not used in the habituation sequences.

Block Structure

All blocks contained 30 sequences and an equal number of the six possible timing templates for habituation sequences. Sequences could not start with the same image as the final fractal of the previous sequence. In deviant blocks, six of the 30 sequences were deviant sequences. Deviant sequences did not occur in the first six sequences (to avoid block initiation) or consecutively. Blocks with two- and six-image sequences contained an equal number of both.

Run Structure

Each run contained five sequence blocks interleaved with 14 s fixation blocks (**Figure 1D**). The first sequence block was always all habituation sequences. The four subsequent sequence blocks each contained one type of deviant sequence. The sequential rule used for each run was counterbalanced across runs and sessions to have an equal number of each. Monkeys typically completed 4-8 runs of this task (among other tasks) in a session.

<u>No Sequence (NoSEQ) Task</u>

The main difference between NoSEQ and SEQ was that images were not arranged according to a sequential rule (as in SEQ) and instead displayed in pseudorandom order such that there were no consecutively repeated images. Images were still displayed as grouped into four-, two-, or six-image sets, depending on the block. All the remaining basic structure of NoSEQ was the same as SEQ. We adjusted the terminology to reflect this fact and more clearly dissociate between the

247 tasks. There were the same 9 timing templates in NoSEQ as in SEQ. However, for NoSEQ,
248 rather than referring to them as 6 habituation and 3 deviant timing templates as in SEQ, we refer
249 to them as 6 standard and 3 nonstandard timing templates in NoSEQ. Similarly, the same two
250 pools of fractal images referred to as habituation and deviant in SEQ are referred to as the 4
251 standard and 3 nonstandard images in NoSEQ. We underscore that the timing templates and
252 image pools are the same between SEQ and NoSEQ within a single scanning session, despite the
253 difference in naming.

254 *Block Types and Structure*

255 We define trials as a series of grouped images with the same timing structure. Most trials
256 contained four images, with some containing two or six (described further below). All blocks
257 contained 30 trials (120 images total). We note that even though images are grouped into trials,
258 reward is on an independent schedule based on the duration of fixation, as in the SEQ task. The
259 first six trials in a block did not contain nonstandard timing templates or nonstandard images.
260 Each block contained key differences with respect to the composition of the timing templates and
261 images used. There were four possible block types (**Figure 1E**), as follows:

262 - *All Standard Timing*: Each four-image trial used one of the 6 possible standard timing
263 templates (5 of each). Images were drawn only from the standard pool. This condition is
264 the same structure as habituation timing in the SEQ task.
265 - *Four-Image Nonstandard Timing (4NST)*: Six trials had four-image nonstandard timing
266 and the remaining 24 trials had standard timing. This timing structure matched the NISR
267 and rule deviant blocks in the SEQ task. The relative fraction of nonstandard images
268 matched the SEQ task (20%, 24 individual images), but they were randomly intermixed
269 with images from the standard pool.

- *Two- and Six-Image Nonstandard Timing (2/6NST)*: Six trials had two- or six-image nonstandard timing (three of each) and the remaining 24 trials had standard timing. This timing structure matched the number deviant blocks in the SEQ task. As in Four-Image Nonstandard Timing blocks, 20% of images were drawn from the nonstandard image pool and the remainder from the standard image pool. All images were displayed in random order.
- *Novel*: As in the Standard Timing block, each four-image trial used one of the 6 possible standard timing templates (5 of each). However, the images came from a novel pool of four images that had not been used in either the standard or nonstandard image pools.

Run Structure

Each run was composed of four image blocks, interleaved with 14 s fixation blocks. The first block of each run was always an All Standard Timing block. The two subsequent blocks were either a Four-Image Nonstandard Timing block or a Two- and Six-Image Nonstandard Timing block, with their order counterbalanced across runs. The last block was always a Novel block. Runs lasted approximately 10 min. Monkeys typically completed 2-4 runs of this task (among other tasks) in a single scanning session.

Data Acquisition

<u>FMRI Data Acquisition</u>

Methods are as described in (Yusif Rodriguez et al., 2023) and briefly summarized here. Monkeys sat in the “sphinx” position in an MR-safe primate chair (Applied Prototype, Franklin, MA or custom-made by Brown University) with their head restrained using a plastic “post” (PEEK, Applied Prototype, Franklin, MA) affixed to the monkeys’ head and the primate chair. Monkeys wore earplugs during MRI scanning (Mack's Soft Moldable Silicone Putty Ear Plugs,

293 “kid’s” size). Monkeys were habituated to all scanning procedures prior to the MRI scanning
294 sessions.
295
296 Approximately 30-60 min prior to each scanning session, monkeys were intravenously injected
297 with a contrast agent: monocrystalline iron oxide nanoparticle (MION, Feraheme (ferumoxytol),
298 AMAG Pharmaceuticals, Inc., Waltham, MA, 30 mg per mL or BioPal Molday ION, Biophysics
299 Assay Lab Inc., Worcester, MA, 30 mg per mL). MION was injected into the saphenous vein
300 below the knee (7 mg/kg), then flushed with a volume of sterile saline approximately double the
301 volume of the MION injected. No additional MION was added during scanning.
302
303 A Siemens 3T PRISMA MRI system with a custom six-channel surface coil (ScanMed, Omaha,
304 NE) at the Brown University MRI Research Facility was used for whole-brain imaging.
305 Anatomical scans consisted of a T1-MPRAGE (repetition time, TR, 2700 ms; echo time, TE,
306 3.16 ms; flip angle, 9°; 208 sagittal slices; 0.5 x 0.5 x 0.5 mm), a T2 anatomical (TR, 3200 ms;
307 TE 410 ms; variable flip angle; 192 interleaved transversal slices; 0.4 x 0.4 x 0.4 mm), and an
308 additional high resolution T2 anatomical (TR, 8020 ms; TE 44 ms; flip angle, 122°; 30
309 interleaved transversal slices; 0.4 x 0.4 x 1.2 mm). Functional images were acquired using a fat-
310 saturated gradient-echoplanar sequence (TR, 1.8 s; TE, 15 ms; flip angle, 80°; 40 interleaved
311 axial slices; 1.1 x 1.1 x 1.1 mm).

312 **Data Analysis**

313 All preprocessing and data inclusion criteria are the same as in (Yusif Rodriguez et al., 2023).
314 Most analyses were performed in Matlab using SPM 12 (https://www.fil.ion.ucl.ac.uk/spm).
315 Prior to analysis, data were preprocessed using the following steps: reorienting (to ensure proper

316 assignment of the x,y,z planes), motion correction (realignment), normalization, and spatial
317 smoothing (2 mm isotropic Gaussian kernel separately for gray matter and white matter). All
318 steps were performed on individual runs separately. The T1-MPRAGE anatomical image was
319 skull stripped using FSL BET brain extraction tool (http://www.fmrib.ox.ac.uk/fsl/) to facilitate
320 normalization. All images were normalized to the 112-RM SL macaque atlas (McLaren et al.,
321 2009).
322
323 Runs were included for analysis only if they met the following criteria: the monkey had to be
324 performing well and a sufficient number of acquisition volumes within the run had to pass data
325 quality checks. The monkey's performance was evaluated by calculating the percentage of time
326 within a run that fixation was maintained. Runs were excluded if the monkey was fixating < 80%
327 of the time. We used the ART toolbox (Artifact Detection Tools,
328 https://www.nitrc.org/projects/artifact_detect) to detect outlier volumes (standard global mean;
329 global signal detection outlier detection threshold = 4.5; motion threshold = 1.1mm; scan to scan
330 motion and global signal change for outlier detection). Any run with greater than 12% of
331 volumes excluded was excluded from analysis (**Table 1**).
332
333 FMRI Models
334 For all models, data were binned to evenly distribute included runs from the SEQ and NoSEQ
335 tasks (**Table 1**) into pseudo-subject bins. Each bin contained data from only one monkey and
336 distributed runs from the SEQ and NoSEQ tasks as evenly as possible. Each bin contained
337 approximately 20 SEQ and 10 NoSEQ runs. Runs from earlier and later scanning sessions were
338 pseudorandomly distributed across bins. For the SEQ task, both rule types (AAAA and AAAB)

were evenly distributed in each bin. This binning procedure resulted in 11 total pseudo-subject bins.

Within-subject statistical models were constructed under the assumptions of the general linear model (GLM) in SPM 12 for each pseudo-subject bin. Condition regressors were all convolved with a gamma function (shape parameter = 1.55, scale parameter = 0.022727) to model the MION hemodynamic response function (Vanduffel and Farivar, 2014). The first six image groups (24 images) and reward times were included as nuisance conditions. Additional nuisance regressors were included for the six motion estimate parameters (translation and rotation) and image variability (standard deviation of within-run image movement variability, calculated using the ART toolbox). Outlier volumes determined with the ART toolbox in preprocessing were "scrubbed" by adding an additional regressors, each with a "1" only at the volume to be excluded.

Regressors were estimated using a bin-specific fixed-effects model. Whole-brain estimates of bin-specific effects were entered into second-level analyses that treated bin as a random effect. One-sample t-tests (contrast value vs zero, $p < 0.005$) were used to assess significance. These effects were corrected for multiple comparisons when examining whole-brain group voxelwise effects using extent thresholds at the cluster level to yield false discovery rate (FDR) error correction ($p < 0.05$).

To assess the univariate effects of deviant sequences, we constructed a general linear model (GLM) using instantaneous stimulus onset regressors. Both tasks were modeled simultaneously,

with runs from both tasks included in each pseudo-subject bin. For the SEQ task, onsets were modeled similarly as described in Yusif Rodriguez, et al. (2023). Onsets were modeled at the first item in each sequence type. Habituation and deviant sequences were modeled separately. Habituation sequences were divided by timing template (short, medium, and long) and whether they came from the first block containing only habituation sequences or a subsequent block that contained deviant and habituation images, yielding six total habituation sequence regressors. Deviant sequences were modeled separately according to their type: NISR, rule deviants, number deviants (two- and six-image), and double deviants (two- and six-image), yielding six total deviant sequence regressors. In total, the SEQ task contained 12 condition regressors (**Table 2**).

For the NoSEQ task, onsets were modeled for the first item in each group of images (a single timing template). Standard and nonstandard timing templates were modeled separately. As in the SEQ task, standard timing templates were divided by those occurring in the first block (where there were no nonstandard timing templates or images) and those occurring in subsequent blocks that contained nonstandard images and timing templates. Standard timing templates were again divided by short, medium, and long yielding a total of six standard timing template regressors. Nonstandard timing templates were modeled separately as four-image and two- and six-image, yielding three total nonstandard timing template regressors. Nonstandard images that were randomly interspersed in blocks that contained nonstandard timing templates were modeled separately at the onset of each individual nonstandard image. The novel image block was also separately modeled and divided by the three standard timing templates (short, medium, long); however, these were not included in analyses. In summary, the NoSEQ task contained six

384 standard time, three nonstandard time, one nonstandard image, and three novel image regressors
385 for a total of 13 regressors (**Table 2**).
386
387 ROI Analysis
388
389 Individual area 46 subregion ROI images were directly acquired from the MEBRAINS
390 Multilevel Macaque Atlas (Balan et al., 2024) (https://www.ebrains.eu/tools/monkey-brain-
391 atlas). Individual subregion image warps were created from their native space to 112RM-SL
392 space using Rhemap (Sirmpilatze and Klink, 2020) (https://github.com/PRIME-RE/RheMAP).
393 Individual warps were then applied to create images used in ROI analysis for p46v (**Figure 2**).
394 Because the ROI used in (Yusif Rodriguez et al., 2023) spanned subregions p46df and p46vf and
395 responses in these subregions were not distinct, for simplicity, we combined subregions in the
396 fundus of area 46 to create p46f (p46df + p46vf).
397
398 To compare activation within and across ROIs in a manner that controlled for variance, we
399 extracted t-values from the condition of interest over baseline using the Marsbar toolbox (Jean-
400 Baptiste Poline, 2002). T-values (one for each pseudo-subject bin: n = 11 bins) were entered into
401 RM-ANOVAs with the identity of the monkey entered as a covariate.

402 **Results**

403
404 We show awake fMRI results from three male monkeys (Macaca mulatta) during two no-report
405 (only central fixation was required) viewing tasks. One was an abstract sequence viewing task
406 (abbreviated SEQ hereafter) that contained a visual sequence rule and structured timing (as

407 reported in Yusif Rodriguez, et al., 2023). The second task did not contain abstract visual
408 sequences (abbreviated NoSEQ hereafter), but maintained the same stimulus frequencies and
409 periodicity structure as SEQ (**Figure 1**). Our main goals were to 1) test if sequential responses
410 differ between the fundus and more ventral LPFC subregions, and 2) test if and how these
411 subregions respond to changes in the components of abstract visual sequences.
412

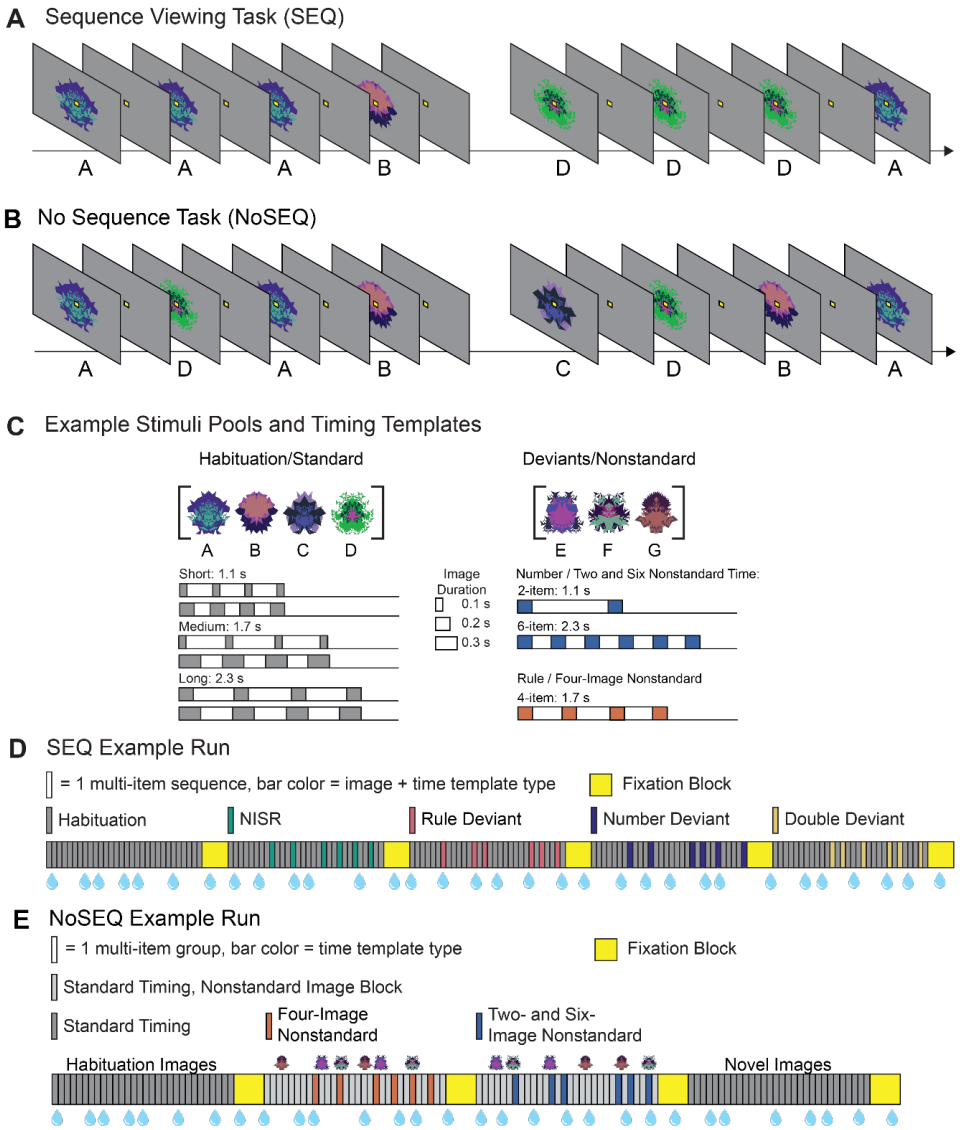

413

414 **Figure 1. Sequence viewing task (SEQ) and No Sequence (NoSEQ) task structure.** Both tasks are no-report. The
415 monkey maintains fixation at the central fixation spot throughout both tasks. **A**. Example partial habituation block

416 from SEQ task for sequence rule three same, one different (AAAB) and habituation timing templates. **B**. Example
417 partial standard block from NoSEQ illustrating non-sequential image order and standard timing templates. **C**.
418 Example stimuli pools (top) show a set of images that would be used in a single scanning session for both tasks (but
419 termed differently depending on the task). NoSEQ additionally contains a novel images category, with different
420 images not exemplified here. New images are used each session. Six possible habituation/standard event timing
421 templates (bottom, left) and deviant/nonstandard event timing templates (bottom, right) illustrated with gray
422 rectangles indicating individual image presentations. Total sequence/grouping durations are listed for each template
423 type. **D**. Example SEQ run, with each bar indicating one multi-image sequence: four images in habituation, new
424 items same rule (NISR), and rule deviants; two or six images in number and double deviants. Each block contains 30
425 sequences. The first block contains only habituation sequences and subsequent blocks (order counterbalanced)
426 contain only one of the four deviant types in six out of the 30 sequences. E. Example NoSEQ run where there is no
427 sequential order to the displayed images. Each bar indicates a multi-image set grouped by timing template and each
428 block contains 30 image groupings. To parallel SEQ structure, the first block in NoSEQ contains only standard
429 images and timing templates. In the two following blocks (order counterbalanced), six out of the 30 groupings have
430 nonstandard timing templates. One block has 4-image nonstandard timing (4NST) that parallels the rule deviant
431 block in SEQ, and the other block has 2- and 6-image nonstandard timing (2/6NST) together to parallel the number
432 deviant block in SEQ. Also, in the nonstandard blocks, 20% of the fractal images shown (in pseudorandom order)
433 are nonstandard (indicated by miniaturized nonstandard fractals), and the rest standard, again to mirror the
434 proportions in SEQ. Task relevant blocks alternate with fixation blocks for both SEQ and NoSEQ tasks. Blue water
435 droplets schematize reward delivery, which is decoupled from sequence viewing and delivered on a graduated
436 schedule based on the duration the monkey has maintained fixation.

437

438 **The fundus of area 46 differentially represents changes to abstract visual sequences**

439 To address our first question, we first tested if sequential responses differed between LPFC
440 subregions: one in the fundus and one adjacent and more ventral. To accomplish this goal, we

441 first needed to define two things: the precise anatomical locations of the regions of interest
442 (ROIs) and sequential responses.
443
444 To define the ROIs, we used a parcellation of PFC in conjunction with our previously defined
445 ROI in Yusif Rodriguez (2023). The previous ROI was a 3 mm radius (895 voxels) sphere in the
446 right hemisphere (named R46) based on coordinates chosen for their functional connectivity
447 similarity to human sequence responsive areas of the lateral frontal cortex (Sallet et al., 2013).
448 This ROI was not conducive to comparing directly adjacent areas because of its spherical shape
449 and because it necessarily included some white matter. Therefore, we created ROIs using the
450 MEBRAINS Multilevel Macaque Brain Atlas (Rapan et al., 2023; Balan et al., 2024) that
451 parcellated PFC according to cytoarchitectonics, functional connectivity, and neurochemical
452 data. This atlas divides area 46 into eight distinct regions (four anterior and four posterior) that
453 are then divided into dorsal and ventral shoulder and fundus regions (**Figure 2A**,**B**). Of the area
454 46 subdivisions, the posterior fundus (p46df and p46vf) regions showed the greatest overlap with
455 the previous R46 ROI constructed from functional connectivity seed coordinates (Sallet et al.,
456 2013; Yusif Rodriguez et al., 2023) (**Figure 2C**). Of the 895 voxels in the previous R46 ROI,
457 40.5% (420) overlapped with cortical gray matter, and all those voxels overlapped with p46df
458 and p46vf combined. We therefore combined the fundus regions and focused our analyses on the
459 posterior fundus (p46f). We compared p46f (1036 voxels) to an adjacent, more ventral
460 subregion: posterior ventral (p46v, 1060 voxels). We focused on ROIs in the right hemisphere
461 because previous results were observed on the right (though the right hemisphere was not
462 statistically different from the left) (Yusif Rodriguez et al., 2023).
463

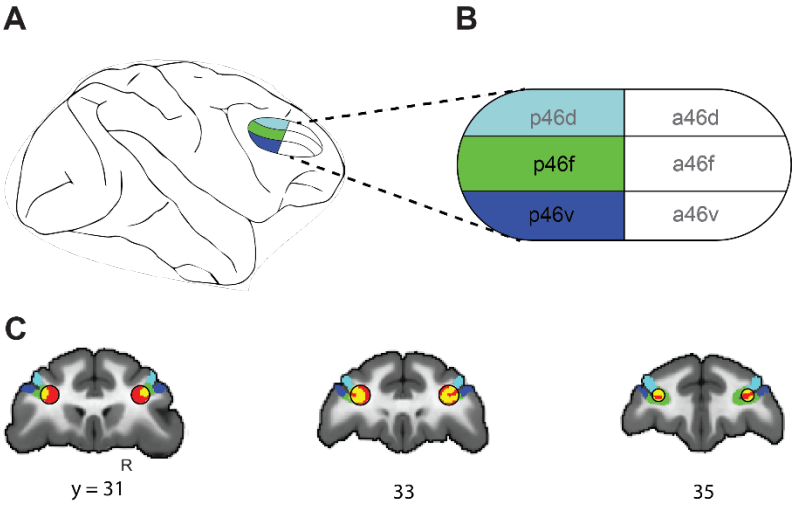

Figure 2. Schematic of anatomical subdivisions of area 46. A. Schematic of the area 46 subregions in the LPFC based on the atlas by Rapan et al. 2023 depicted on the right lateral surface of the macaque brain. **B.** Same cortical subregions illustrated in **A** with areas of comparison p46f and p46v in green and blue. Area p46d (light blue) shown only for context, indicated by gray lettering. **C.** Coronal slices displaying the area 46 ROI sphere used in Yusif Rodriguez et al. 2023 (red, outlined in black) superimposed on area 46 subregions. ROIs used for analysis in this study were green and blue, corresponding to regions illustrated in **A**). Light blue p46d only included for comparison and not used in analyses. Yellow voxels indicate overlap between the previous red sphere and current p46f ROI (green).

To define sequential responses, we used deviations from an established (habituated) abstract visual sequence in the SEQ task (as in (Yusif Rodriguez et al., 2023)). The general logic was that regions that responded to changes in the abstract visual sequence may play a role in tracking that information. To create these changes, monkeys were first habituated to four-item sequences of images that followed a particular rule, e.g., same, same, same, different. Images were drawn from a pool of habituation images. In subsequent blocks, some of the sequences (6 out of 30) were deviant sequences that drew images from a separate deviant pool and differed from habituation sequences in one of four ways: new items, same rule (NISR), rule deviants, number

482 deviants, or double deviants (included to counterbalance the design but not included for
483 analysis). All comparisons to determine abstract sequence responses in the SEQ task were
484 between NISR and rule or number deviants. This comparison controlled for the use of less
485 frequent deviant images and any changes observed would be due to changes in the abstract
486 sequence.
487
488 For all analyses, we measured the cerebral blood volume (CBV) of a contrast agent,
489 monocrystalline iron oxide nanoparticle (MION) activity as our indicator of neural activity. We
490 created a single model for both the SEQ and NoSEQ tasks (see Methods for details). Statistical
491 testing was performed on approximately 20-run bins (n = 11), each consisting of data from a
492 single monkey. For each condition, t-values were extracted for that condition compared to
493 baseline (e.g., Rule Deviant > Baseline) to account for potential differences in variance across
494 conditions. These values were used to examine ROI activity throughout, and we refer to
495 comparisons by the condition of interest (i.e., without listing the contrast over baseline, e.g., Rule
496 Deviant). All statistical tests on ROIs were performed on binned data and included a covariate
497 for monkey identity (n = 3). While we report the effect of variation between monkeys in the
498 following analyses, the main focus of the study was not on individual differences, and our
499 discussion focuses on condition effects.
500
501 We first tested the hypothesis that sequential responses differ between right p46f and p46v. As in
502 our previous study, we compared the sequence deviants Rule and Number to NISR, with
503 increased activity for deviants indicating sequential processing. Replicating previous results
504 (with the newly defined ROI), both deviant responses were significantly greater than NISR in
505 right p46f (Rule > NISR: p = 0.01; Number > NISR: p = 0.04, **Figure 2A,B**, **Table 3**). In

contrast, responses in p46v did not differ between deviants and NISR, resulting in a significant interaction between the two areas for number deviants compared to NISR (p = 0.02, **Figure 2B**, **Table 4**) and a marginal interaction for rule deviants compared to NISR (p = 0.09, **Figure 2A**, **Table 4**). These ROI results were supported by whole brain contrasts of Rule Deviants > NISR (**Figure 2C**) and Number Deviants > NISR (**Figure 2D**) in the SEQ task (**Table 5**). Both deviant types showed significant clusters of activation in right p46f. Therefore, these results support the hypothesis that sequential responses differ between p46f, which responds to changes in abstract visual sequences, and p46v, which does not.

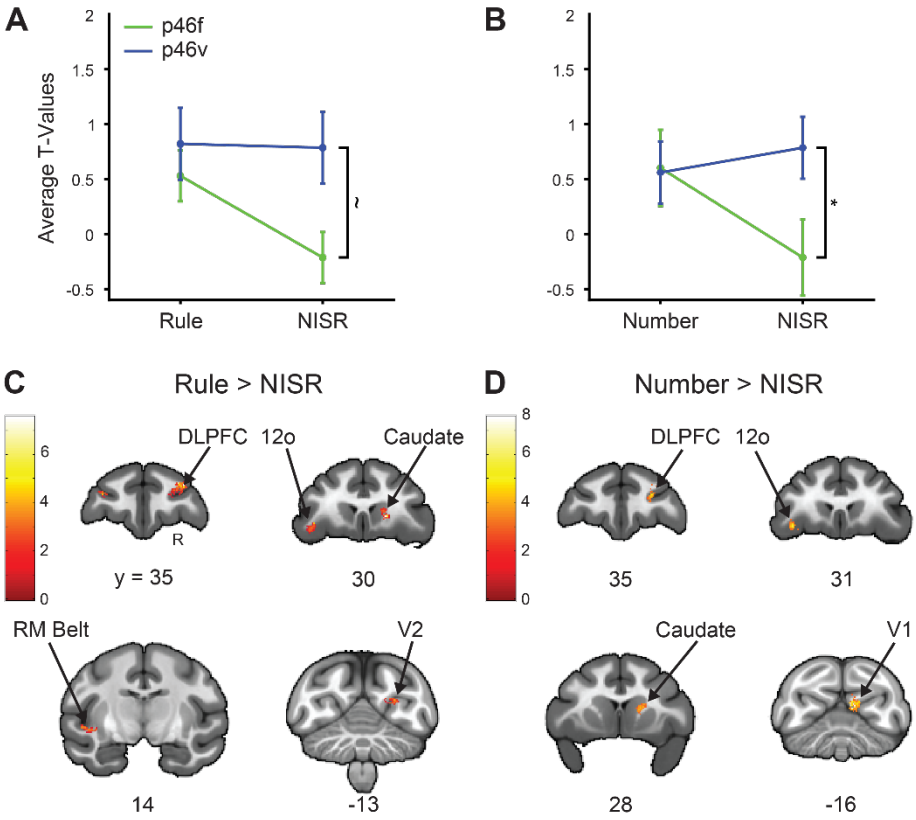

Figure 3. **Right p46f and not p46v showed deviant responses in SEQ task. (A and B)** T-values for the condition of interest > baseline are shown. Error bars are 95% confidence intervals (1.96 x standard error of the within-bin mean). **A**. Responses in rule deviants compared to new items, same rule (NISR) were different between p46f and p46v such that there was a significant main effect of ROI, and a marginal interaction between ROI and condition

520 (indicated with ~). **B**. Number deviants compared to NISR between p46f and p46v showed a marginal main effect of
521 ROI and significant interaction between ROI and condition. **C**. Voxel-wise contrast of Rule Deviants > NISR, false
522 discovery rate (FDR) error cluster corrected for multiple comparisons (FDRc < 0.05, height p < 0.005 unc., extent =
523 100) are shown. D. Voxel-wise contrast of Number Deviants > NISR (FDRc < 0.05, height p < 0.005 unc., extent =
524 133) is shown. Color bar indicates T-values in **C** and **D**.

525

526 **The ventral shoulder of area 46 differentially represents changes to abstract sequence**
527 **components**

528 We next addressed the second question of if and how these regions respond to changes in
529 sequential components in the absence of an abstract visual sequence. We examined two main
530 features in the NoSEQ task: image periodicity (timing template) and identity. These two image
531 features are components of the SEQ task, exist in parallel in the NoSEQ task, and will be
532 described further below.

533

534 To test for responses in the DLPFC related to image periodicity, we compared standard to
535 nonstandard timing templates in the NoSEQ task. Previous studies showed that regions of the
536 frontal cortex process different types of timing structures (Onoe et al., 2001; Genovesio et al.,
537 2006; Chiba et al., 2021), raising the possibility that a difference in the timing structure alone
538 could be a component of sequence responses. In the context of this experiment, image periodicity
539 refers to the timing template used. In the SEQ and NoSEQ tasks, most sequences/groups had one
540 of six possible standard timing templates (referred to as habituation in the SEQ task, **Figure 1**).
541 A unique timing template (0.2 s image duration for medium, 1.7 s, total duration) was used
542 infrequently for deviants in the SEQ task (after the first block, 6 out of 30 sequences). In the

543 NoSEQ task that structure was mirrored: after the first block, 6 out of the 30 stimulus groupings
544 used a nonstandard timing template. These blocks either contained six 4-image nonstandard
545 timing (4NST) or three each of 2- and 6-image nonstandard timing (2/6NST). Importantly, even
546 though the timing template was the same as for SEQ deviants (just termed differently for the
547 NoSEQ task), the images in NoSEQ were pseudorandomly presented and were not composed of
548 entirely nonstandard images. To determine if brain areas responded to changes in timing
549 template alone, we compared responses to these nonstandard timing templates to the six other
550 standard timing templates in the NoSEQ task.
551
552 We tested the hypothesis that p46v would show a greater difference in responses to image
553 periodicity than p46f in the NoSEQ task. In general, more ventral LPFC regions are thought to
554 have more object-based or visual responses (Meyer et al., 2011; Yamagata et al., 2012; Tang et
555 al., 2021; Xu et al., 2022). First, we found that changes in timing structure alone did not elicit
556 deviant responses in right p46f. There were no reliable differences between 4NST ($p = 0.86$,
557 **Figure 4A**, **Table 6**) or 2/6NST compared to standard timing templates ($p = 0.85$, **Figure 4B**,
558 **Table 6**). In contrast, right p46v showed reliable differences when comparing standard to 4NST
559 ($p = 0.03$, **Figure 4A**, **Table 6**) and standard to 2/6NST ($p = 0.01$, **Figure 4B**, **Table 6**). When
560 directly comparing p46f and p46v, overall responses were greater in p46v than p46f ($p = 0.01$,
561 **Table 7**) and there was a significant interaction such that the difference between nonstandard and
562 standard was significantly different by ROI for 2/6NST and marginal for 4NST (ROI x
563 condition, 2/6NST: $p = 0.05$, 4NST: $p = 0.09$; **Table 7**). These results were supported by whole
564 brain contrasts of 4NST > Standard Timing and 2/6NST > Standard Timing showing no
565 significant clusters of activation in p46f with other significant activation in distinct visual and

association areas (**Figure 4C,D**, **Table 8**). Together, these results support the hypothesis that p46v responds to image periodicity and dissociates from responses in p46f. Further, p46v may be part of a network of other brain areas that is specialized to detect periodicity differences, independent of abstract sequential structure.

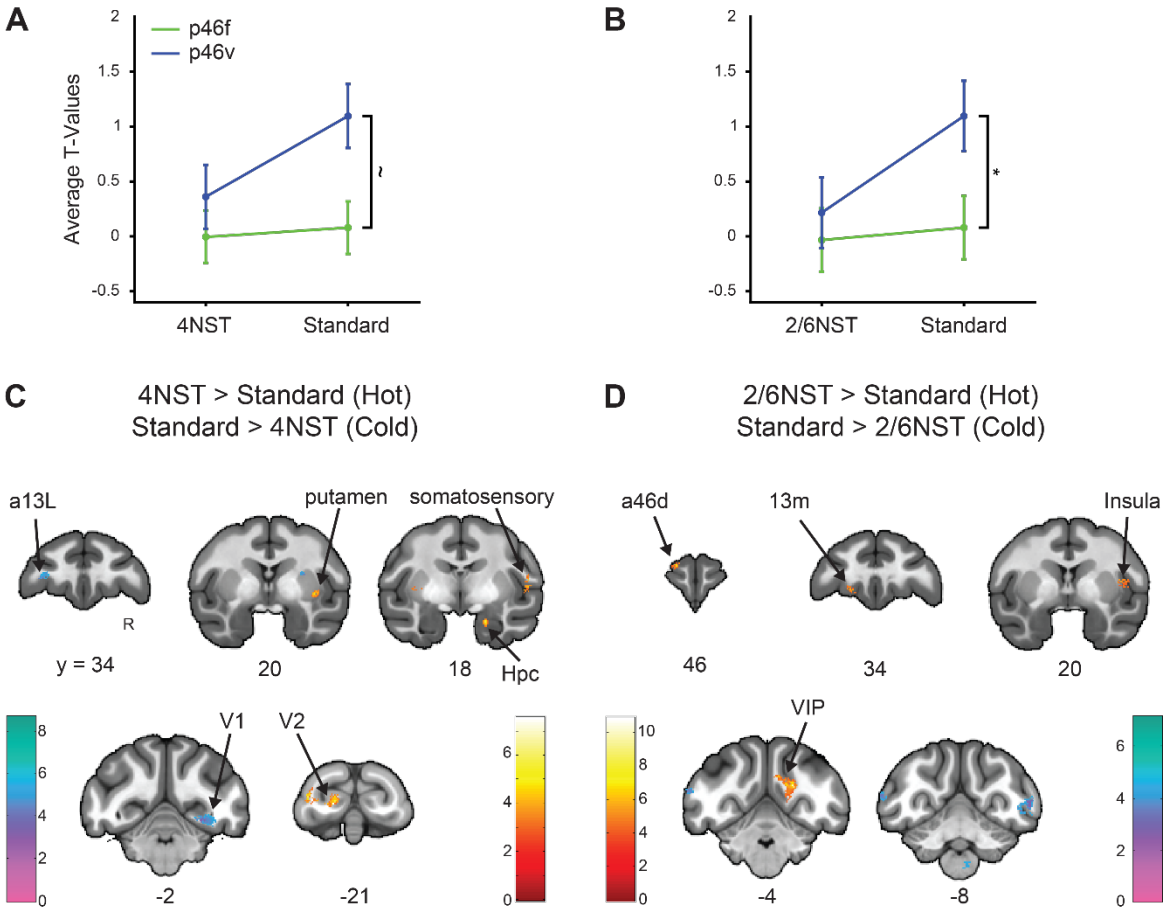

Figure 4. Right p46v and not p46f showed different responses to timing templates in NoSEQ. (A and B) T-values for the condition of interest > baseline are shown. Error bars are 95% confidence intervals (1.96 x standard error of the within-bin mean). **A.** 4NST compared to standard timing between p46f and p46v shows a significant main effect of ROI and a marginal interaction between ROI and condition (indicated with ~). **B**. 2/6NST compared to standard between p46f and p46v shows a significant main effect of ROI and interaction between ROI and condition (indicated with *). **C.** Voxel wise contrasts of 4NST > Standard timing (Hot colors) false discovery rate (FDR) error cluster corrected for multiple comparisons (FDRc < 0.05, height p < 0.005 unc., extent = 84), overlaid

with Standard timing > 4NST (Cold colors) false discovery rate (FDR) error cluster corrected for multiple comparisons (FDRc < 0.05, height p < 0.005 unc., extent = 204) are shown. **D.** Voxel wise contrasts of 2/6NST > Standard timing (hot colors; FDRc < 0.05, height p < 0.005 unc., extent = 94), overlaid with Standard timing > 2/6NST (cold colors; FDRc < 0.05, height p < 0.005 unc., extent = 104) are shown. Color bars indicate T-values in **C** and **D**.

To test for responses in the LPFC related to image identity, we compared standard to nonstandard images in the NoSEQ task. Deviant/nonstandard images in the SEQ task were less frequent. It is unlikely that the deviant responses observed in the SEQ task were driven by these images, because deviant comparisons were all made across conditions that contained images from the deviant pool (e.g., rule deviant vs. NISR, **Figure 1**). However, infrequent or surprising images have been shown to drive responses in LPFC (Chao et al., 2018; Camalier et al., 2019; Grohn et al., 2020). Therefore, we aimed to determine if responses in area 46 could be driven by less frequent image presentations, independent of sequential context. To examine this sequence component, we again used conditions that were separate from an abstract visual sequence, i.e., in the NoSEQ task. We compared responses to the randomly interspersed nonstandard images to standard images to ensure other aspects of the task were held constant.

We tested the hypothesis that p46v would show a greater difference in responses to image identity than p46f in the NoSEQ task. First, we found that nonstandard responses were not reliably different from standard image responses in right p46f (p = 0.67, **Figure 5A**, **Table 9**). In contrast, p46v differentiated between standard and nonstandard images, but with reliably greater responses for standard images (p = 0.01, **Figure 5A**, **Table 9**). We directly compared responses in p46f to p46v and found that responses to nonstandard compared to standard images were

603 reliably different (ROI x condition: p = 0.03, **Table 10**). These ROI results showing greater
604 responses to standard than nonstandard images were also supported by whole brain contrasts
605 (**Figure 5B**). Significant clusters of activation were observed for Standard > Nonstandard images
606 in right p46v but no other area 46 subregions (**Table 11**). In Nonstandard > Standard image there
607 were no significant clusters in the frontal cortex. These results support the hypothesis that p46v
608 differentially represents standard and nonstandard images, and p46f does not.
609

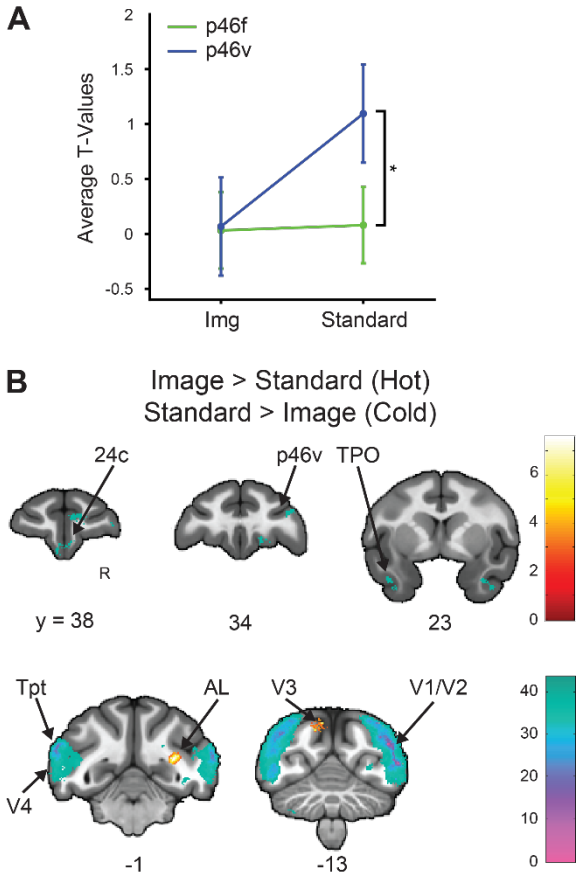

610

611 **Figure 5. Right p46v and not p46f shows different responses to standard and nonstandard images in the**
612 **NoSEQ task.** T-values for the condition of interest > baseline are shown. Error bars are 95% confidence intervals
613 (1.96 x standard error of the within-bin mean). **A.** Nonstandard compared to standard images showing reliable
614 differences between p46f and p46v showing a significant main effect of ROI with a significant interaction of ROI
615 and condition (indicated with *). **B.** Voxel wise contrasts of Nonstandard > Standard images false discovery rate

(FDR) error cluster corrected for multiple comparisons (hot colors, FDRc < 0.05, height p < 0.005 unc., extent = 101), overlaid with Standard > Nonstandard image (cold colors, FDRc < 0.05, height p < 0.005 unc., extent = 88) are shown. Color bar indicates T-values.

Discussion

We had two main goals in this experiment: 1) to test if SEQ deviant responses previously observed in p46f were different from those in p46v, and 2) to test if and how p46f and p46v responded to changes in abstract visual sequence components, image identity and periodicity, alone in a NoSEQ task. We hypothesized that p46v would not respond to changes in abstract visual sequences as a whole, but to the defined components. The results generally supported the hypotheses, with p46f responding more strongly than p46v to abstract sequence deviants in the SEQ task but not to differences in sequential components (standard vs nonstandard) in NoSEQ, further strengthening its role as an area that uniquely represents abstract sequential changes. P46v instead differentiated between standard and nonstandard sequence components, image identity and periodicity, in NoSEQ. This result supported our predictions that this region was more influenced by visual sensory inputs and not necessarily the higher order structures in abstract sequences. These results provide important knowledge of the functional subdivisions within area 46 of the LPFC and scaffold future understanding of this important area for cognition.

638 The observed differences between p46f and p46v may expand on the notion of "dorsal" and
639 "ventral" distinctions within the LPFC. Classic anatomical definitions of dorsal and ventral have
640 used the principal sulcus as a dividing line, bisecting the fundus between the two (e.g., (Petrides
641 and Pandya, 1999)). Extracellular electrophysiology experiments often focus on the cortical
642 surface of LPFC, understandably due to the ability to visualize locations and position electrodes
643 and arrays. Therefore, it is less clear how the fundus region itself may or may not fit into
644 functional generalizations of LPFC. Anatomy and the present experiment suggest a more distinct
645 functional role for p46f, at least within more posterior LPFC regions. The present results
646 strikingly align with a multimodal parcellation of macaque area 46 showing that p46f
647 hierarchically clustered with the most rostral regions of LPFC whereas p46v clustered with more
648 caudal sensory and motor areas (Rapan et al., 2023). Current schema of the functional
649 organization of LPFC suggest that more spatial and action-oriented responses are localized more
650 dorsally and more non-spatial and object oriented responses are localized more ventrally (Meyer
651 et al., 2011; Yamagata et al., 2012; Tang et al., 2021; Xu et al., 2022). Further, we did not
652 observe responses to changes in abstract visual sequences in p46v, as others have observed in
653 what was termed VLPFC (Wang et al., 2015; Bellet et al., 2024). It is unclear if p46v and
654 VLPFC are anatomically overlapping. More experiments are needed before strong conclusions
655 can be drawn, but the results here suggest that the subregions within what has been referred to as
656 DLPFC and VLPFC should be carefully considered, and the fundus may need separate
657 classification. Future experiments could benefit from recent developments in whole brain
658 imaging technology including functional contrast agents, PET-MR, and high field fMRI to
659 localize anatomical and functional brain regions both independently and pre/post-
660 electrophysiological recordings.

We did not observe responses in p46f to changes in the periodicity alone in NoSEQ. In contrast, right p46v showed differences in responding to standard and nonstandard timing templates, with increased responses to the more frequent standard timing presentations. These observations are generally consistent with previous observations of timing-related activity in monkey LPFC (Niki and Watanabe, 1979; Onoe et al., 2001; Genovesio et al., 2006; Cueva et al., 2020; Chiba et al., 2021), although the precise anatomical location was not specified. Human LPFC responses in temporal expectation tasks (Coull and Nobre, 2008) were also similar. Outside of area 46 we observed some of the same regions that have been observed for duration perception in monkeys, such as putamen, cerebellum, and V2 (Onoe et al., 2001). We also observed regions similar to those observed in humans related to temporal expectation such as the basal ganglia, temporal cortex, and cerebellum (Coull and Nobre, 2008). Together these results illustrate the specificity of subregions within area 46 and suggest that adjacent subregions code for different stimulus properties.

Area p46v responses differentiated between standard and nonstandard images in NoSEQ while p46f did not. Responses in p46v were greater to standard images than nonstandard images. These results suggest that this response was not a typical ‘surprise’ response. In our task, standard images were presented with greater frequency, and closer in time to each other, than the isolated individual appearances of the nonstandard images. Therefore, such responses could be partially driven by the increased frequency, and thus a greater summed BOLD response, of standard compared to nonstandard images and. This increased image frequency may have been the primary driver of responses in regions such as visual cortex, which showed relatively large

684 significant clusters in Standard > Nonstandard NoSEQ images. However, if frequency was the
685 only driver of such responses, then we would have likely observed these responses throughout
686 the whole brain rather than in a specific set of regions. Outside of the visual cortex there were
687 roughly equal numbers of areas that showed responses to the reverse contrast (Nonstandard
688 Image > Standard Image), but these responses were not located in area 46. An intriguing
689 possibility is that a greater response to the standard images in p46v is due to the previous
690 association that those images have to abstract visual sequences, or their greater familiarity
691 (Rainer et al., 1999; Stern et al., 2001; Leaver et al., 2009). Further investigation will be
692 necessary to determine if that association is a component of the response in p46v along with
693 regions observed for Standard Image > Nonstandard Image in the whole brain. There were a
694 small number of regions observed outside of the frontal cortex that showed significantly greater
695 responses to nonstandard images. These regions were not necessarily overlapping with areas
696 typically associated with 'surprise' or prediction error (Grohn et al., 2020), again raising the
697 prospect that a form of association may govern these responses as well. Further research will be
698 needed to discern the underlying driving forces, but the fact remains that sensory related
699 responses localize to p46v and not adjacent p46f, again illustrating the specificity of responses
700 within area 46.
701
702 This study's approach was limited in the following ways. First, though p46f and p46v showed
703 significant differences, some effect sizes remained small. These results could be related to
704 limitations of whole-brain event-related monkey fMRI: the spatial resolution, signal-to-noise,
705 and inherent smoothness of the data. There could be differences in alignment of the voxels with
706 the regions and partial volume effects that would be difficult to resolve without fundamentally

707 changing the experiment by scanning a small volume at higher resolution, using a greater field
708 strength (which may not be available), or greatly increasing the sample size (introducing other
709 limitations). However, these experiments provide an ideal foundation for techniques with higher
710 spatial resolution such as electrophysiological recordings. Second, while the no-report paradigm
711 confers the advantage of eliminating possible confounds due to executing responses, it does not
712 allow for direct comparisons with behavior performance. In other words, even though we have
713 observed that regions within area 46 respond to changes in stimuli, we do not know how such
714 information may contribute to decisions or the production of actions. Third, we have specifically
715 focused on two subregions within area 46, which is itself only one of several areas defined as
716 belonging to LPFC. Other regions within and beyond LPFC warrant further investigation, and
717 the results here potentially contextualize further differences within and among subregions.
718 Though some of the preceding items are limitations of the chosen task and technique, we hope
719 that this experiment and others like it highlights the utility of different data acquisition modalities
720 and opens important avenues of future research.
721
722 In conclusion, we provide unique evidence for the anatomical and functional specificity of
723 abstract visual sequence responses in a specific subregion of LPFC, p46f. In tandem, we provide
724 evidence for an adjacent area, p46v, responding to the components of abstract visual sequences.
725 These results reinforce the potential parallel with findings in human brain areas. Rostrolateral
726 PFC in humans is necessary for abstract task sequences and is most analogous to p46f in
727 monkeys (Desrochers et al., 2015; Yusif Rodriguez et al., 2023). Further, these results illustrate
728 the utility in using fMRI to isolate components to cognitive processes, in this case, sequential
729 components. The LPFC, which may have in the past appeared to be a more homogenous region,

730 may in fact be even more distinct in its subdivisions and functional mapping. This study lays the
731 foundation for an approach to functionally dissociating subregions in the cortical structures that
732 underlie many complex and abstract daily functions, such as cooking a meal or appreciating a
733 piece of music.
734

Tables

Table 1. Data excluded and included for analysis.

Percent Excluded Fixation

	Monkey B	Monkey J	Monkey W
SEQ	6.89%	10.46%	3.03%
NoSEQ	5.06%	6.96%	10.13%

Percent Excluded Motion

	Monkey B	Monkey J	Monkey W
SEQ	15.15%	0%	0.6%
NoSEQ	1.89%	16.5%	0.63%

Total Included Runs

	Monkey B	Monkey J	Monkey W	Total Runs
SEQ	70	65	97	232
NoSEQ	17	38	43	98

Table 2. Regressors used in SEQ and NoSEQ model. Both tasks are modeled together.

SEQ Task Regressors	
First Block	**Subsequent Blocks**
Habituation Short	Habituation Short
Habituation Medium	Habituation Medium
Habituation Long	Habituation Long
	New Item Same Rule (NISR)
	Rule Deviant
	Number Deviant – 2 items
	Number Deviant – 6 items
	Double Deviant – 2 items
	Double Deviant – 6 items
NoSEQ Task Regressors	
First Block	**Subsequent Blocks**
Standard timing - Short	Standard timing - Short
Standard timing - Medium	Standard timing - Medium
Standard timing - Long	Standard timing - Long
	Nonstandard image
	4-image nonstandard timing
	2-image nonstandard timing
	6-image nonstandard timing
	Novel image, standard timing - Short
	Novel image, standard timing - Medium
	Novel image, standard timing - Long

Table 3. Activity during SEQ task deviants compared to NISR in right area 46 using repeated measures ANOVAs. P-values in bold are conditions of interest.

Rule Deviant					
	Factor	DFs	F	p	η_p^2
46f	monkey	2,8	1.2	0.36	0.22
	condition	1,8	12.3	**0.01**	0.61
	monkey:condition	2,8	4.6	0.05	0.54
46v	monkey	2,8	4.5	0.05	0.53
	condition	1,8	0	0.93	0
	monkey:condition	2,8	0.2	0.82	0.05
Number Deviant					
	Factor	DFs	F	p	η_p^2
46f	monkey	2,8	0.6	0.57	0.13
	condition	1,8	5.8	**0.04**	0.42
	monkey:condition	2,8	5.5	0.03	0.58
46v	monkey	2,8	2.8	0.12	0.41
	condition	1,8	0.3	0.58	0.04
	monkey:condition	2,8	0.1	0.88	0.03

Table 4. Comparisons of activity in right p46f and p46v during deviants compared to NISR in the SEQ task using repeated measures ANOVAs. P-values in bold are conditions of interest.

Rule Deviant				
Factor	DFs	F	p	η_p^2
monkey	2,18	0.2	0.82	0.02
ROI	1,18	5	0.04	0.22
condition	1,18	2.9	0.11	0.14
monkey:condition	2,18	1.9	0.17	0.18
ROI:condition	1,18	3.3	**0.09**	0.15
Number Deviant				
Factor	DFs	F	p	η_p^2
monkey	2,18	0.6	0.57	0.06
ROI	1,18	3.7	0.07	0.17
condition	1,18	1	0.32	0.05
monkey:condition	2,18	2.5	0.11	0.22
ROI:condition	1,18	6	**0.02**	0.25

749 **Table 5.** Coordinates of activity clusters in Rule and Number deviant > NISR contrasts in the SEQ task.

Contrast Location	Extent (vox)	Peak T-val	X	Y	Z
Rule Deviant > NISR					
Rostral Medial Frontal Pole	105	6.25	0.5	45.5	14.5
Dorsal Area 46	381	7.53	14	35.5	25.5
Ventral Area 46	100	5.53	-15	35.5	22
Medial Agranular Insular Region	159	7.53	8	30.5	15
Orbital Area 12	148	5.59	-18	30.5	12.5
Area F5 of Ventral Pre-motor Cortex	173	6.06	-19	13	9.5
Granular Layer of Dentate Gyrus	137	5.66	-9.5	2.5	12.5
Cerebellum	229	4.85	6	-5.5	5.5
Visual Area 2	123	5.65	12	-12	20
	115	7.21	3	-22	23
Number Deviant > NISR					
Dorsal Area 46	166	5.73	11	36.5	25.5
Orbital Area 12	133	5.17	-18	31	10.5
Medial Area 13	162	5.21	7.5	27.5	17.5
Visual Area 2	332	7.99	5	-17	18

750

751

752 **Table 6.** Activity during NoSEQ task 4NST and 2/6NST compared to standard timing in right area 46 using

753 repeated measures ANOVAs. P-values in bold are conditions of interest.

4NST					
	Factor	DFs	F	p	eta2p
46f	monkey	2,8	0.8	0.5	0.16
	condition	1,8	0	0.86	0
	monkey:condition	2,8	0.1	0.95	0.01
46v	monkey	2,8	9.6	0.01	0.71
	condition	1,8	6.8	**0.03**	0.46
	monkey:condition	2,8	5.1	0.04	0.56
2/6NST					
	Factor	DFs	F	p	eta2p
46f	monkey	2,8	0.1	0.95	0.01
	condition	1,8	0	0.85	0
	monkey:condition	2,8	1.1	0.37	0.22
46v	monkey	2,8	14.5	0	0.78
	condition	1,8	10	**0.01**	0.55
	monkey:condition	2,8	4.4	0.05	0.52

754

Table 7. Comparisons of activity in right p46f and p46v during nonstandard compared to standard timing in the NoSEQ task using repeated measures ANOVAs. P-values in bold are conditions of interest.

4NST				
Factor	DFs	F	p	η_p^2
monkey	2,18	6.3	0.01	0.41
ROI	1,18	8.4	**0.01**	0.32
condition	1,18	2.8	0.11	0.14
monkey:condition	2,18	1.9	0.19	0.17
ROI:condition	1,18	3.1	**0.09**	0.15
2/6NST				
Factor	DFs	F	p	η_p^2
monkey	2,18	3.4	0.06	0.27
ROI	1,18	8.2	**0.01**	0.31
condition	1,18	5.3	0.03	0.23
monkey:condition	2,18	5	0.02	0.36
ROI:condition	1,18	4.3	**0.05**	0.19

Table 8. Coordinates of activity clusters in 4NST and 2/6NST > Standard timing contrasts in the NoSEQ task.

Contrast Location	Extent (vox)	Peak T-val	X	Y	Z
4NST > Standard timing					
Putamen	135	6.8	15.5	22.5	10.5
Temporal Parietooccipital Associated Area	113	5.71	-16	22.5	2
Secondary Somatosensory Cortex	92	6.31	25	18	14
Amygdala	85	5.03	8.5	17.5	1.5
Putamen	137	5.33	-15	15.5	13
Areas 1 and 2	84	4.69	-24	12.5	21
Visual Area 2	192	5.77	-12	-5.5	14
Cerebellum	112	6.1	-8	-9.5	10
Visual Area 2	150	5.26	-14	-18	10.5
Primary Visual Cortex	184	6.63	-6	-22	18.5
Primary Visual Cortex	197	5.44	-16	-22	18.5
Standard timing > 4NST					
Lateral Area 13	204	6.61	-15	33.5	18
Putamen	227	5.45	12.5	21	19
Area 29	494	7.43	16	0	12
2/6NST > Standard timing					
Dorsal Area 46	142	5.75	-7.5	45	22.5
Intermediate Agranular Insula Area	144	6.37	-11	32	9
Area F5 of Ventral Premotor Cortex	94	7.27	26	27	17.5
Agranular and Dysgranular Insula	177	6.52	21	22	15
Area TEm	222	11	-25	8	7
		3.92	-20	4.5	2
Ventral Intraparietal Area	119	4.76	8.5	5	26
Area Pga	244	6.73	-18	4	16.5
Medial Superior Temporal Area	252	6.09	-14	-1	22
Posterior Intraparietal Area	604	6.9	9.5	-5	22.5
Standard timing > 2/6NST					
Area F5 of Ventral Premotor Cortex	123	4.65	-21	29	17.5
Putamen	137	4.57	12	27.5	10.5
Putamen	110	5.16	-17	8.5	12
Temporal Parietooccipital Associated Area	141	6.34	22.5	5	14
Dorsal Visual Area 4	171	7.22	-28	-0.5	17.5
Dorsal Visual Area 4	183	5.95	-28	-4.5	21.5
Lateral Reticular Nucleus	104	4.58	5.5	-7	-4
Primary Visual Cortex	504	6.36	25.5	-7.5	16.5
Primary Visual Cortex	215	5.22	21.5	-12	20.5
Primary Visual Cortex	192	5.29	-20	-13	26

Table 9. Activity during NoSEQ task nonstandard images compared to standard images in right area 46 using repeated measures ANOVAs. P-values in bold are conditions of interest.

	Factor	DFs	F	p	η_p^2
46f	monkey	2,8	1.3	0.32	0.25
	condition	1,8	0.2	0.67	0.02
	monkey:condition	2,8	3.3	0.09	0.45
46v	monkey	2,8	9.7	0.01	0.71
	condition	1,8	11.8	**0.01**	0.6
	monkey:condition	2,8	10.2	0.01	0.72

Table 10. Comparisons of activity in right p46f and p46v during standard compared to nonstandard images in the NoSEQ task using repeated measures ANOVAs. P-values in bold are conditions of interest.

Factor	DFs	F	p	η_p^2
monkey	2,18	1.8	0.2	0.17
ROI	1,18	8.7	0.01	0.33
condition	1,18	7	0.02	0.28
monkey:condition	2,18	12	0	0.57
ROI:condition	1,18	6	**0.03**	0.25

Table 11. Coordinates of activity clusters in Nonstandard Image > Standard Image and Standard Image > Nonstandard Image contrasts in the NoSEQ task.

Contrast Location	Extent (vox)	Peak T-val	X	Y	Z
Nonstandard Image > Standard Image					
Hypothalamus	139	5.12	2	15.5	8.5
Middle Temporal Area	374	7.21	10	3	18
		4.83	17	-2.5	20.5
Ventral Visual Area 4	134	7.09	20	-7.5	8.5
Ventral Visual Area 6A	172	5.83	-3	-14	32
Visual Area 2	101	6.3	-7.5	-15	16.5
		4.06	-3	-20	12
Standard Image > Nonstandard Image					
Caudal Medial Frontal Pole	302	5.93	0	40	10.5
Dorsal Area 46	294	6.05	7	37.5	19
		4.84	7.5	45.5	21.5
Medial Area 13	217	7.08	6.5	34.5	12.5
Ventral Area 46	268	6.27	17.5	34.5	23.5
Area 45b	105	4.08	-20	29	22
Area F5 of Ventral Premotor Cortex	146	5.82	22	27.5	12
STS Part of Temporal Pole	339	5.97	15	24.5	-1.5
		3.25	18	17	-3
Anterior Ventral Area TE	472	7.53	-19	21	-2.5
Putamen	568	6.67	13	19	17
		3.41	8	14.5	21.5
Caudal Dorsal Premotor Cortex	187	6.79	17.5	18	31
Area TEm	344	6.17	23.5	9	9
		5.39	18	11.5	3.5
Temporal Parietooccipital Associated Area	171	5.01	-25	5.5	15.5
Medial Pulvinar Nucleus	93	5.09	-5.5	4.5	17.5
Primary Motor Cortex	88	5.35	11	1.5	31
Ventral Visual Area 4	304	5.32	18.5	-0.5	12
Posterior Intraparietal Areas	150	5.39	-11	-4.5	20.5
Visual Area 2	25046	43.43	19	-11	24
		30.66	23.5	-14	17.5
		21.88	28	0.5	21
		17.48	15.5	-15	30.5
		16.25	25	-5	14
		11.1	25.5	-6	25
		10.18	28	3	13
		8.78	11.5	-3	22.5
		6.57	16.5	-19	12.5
		6.35	18.5	-19	22.5
		5.11	13	-13	16.5

		4.97	3.5	-4.5	24
		4.51	16	-5	15.5
		4.16	26.5	6.5	5.5
Visual Area 2	21128	33.77	-20	-11	30
		24.6	-26	-4	20.5
		18.87	-21	-8.5	14
		17.13	-20	-15	21.5
		14.89	-13	-14	32.5
		6.23	-29	0.5	13.5
		6.15	-20	-20	12.5
		4.56	-14	-19	25.5
Cerebellum	205	5.82	-13	-11	-1.5

References

Balan PF, Zhu Q, Li X, Niu M, Rapan L, Funck T, Wang H, Bakker R, Palomero-Gallagher N, Vanduffel W (2024) MEBRAINS 1.0: A new population-based macaque atlas. Imaging Neuroscience 2:1–26.

Bellet ME, Gay M, Bellet J, Jarraya B, Dehaene S, van Kerkoerle T, Panagiotaropoulos TI (2024) Spontaneously emerging internal models of visual sequences combine abstract and event-specific information in the prefrontal cortex. Cell Rep 43:113952.

Camalier CR, Scarim K, Mishkin M, Averbeck BB (2019) A Comparison of Auditory Oddball Responses in Dorsolateral Prefrontal Cortex, Basolateral Amygdala, and Auditory Cortex of Macaque. Journal of Cognitive Neuroscience 31:1054–1064.

Chao ZC, Takaura K, Wang L, Fujii N, Dehaene S (2018) Large-Scale Cortical Networks for Hierarchical Prediction and Prediction Error in the Primate Brain. Neuron 100:1252-1266.e3.

Chiba A, Morita K, Oshio K, Inase M (2021) Neuronal activity in the monkey prefrontal cortex during a duration discrimination task with visual and auditory cues. Sci Rep 11:17520.

Coull JT, Nobre AC (2008) Dissociating explicit timing from temporal expectation with fMRI. Current Opinion in Neurobiology 18:137–144.

Cueva CJ, Saez A, Marcos E, Genovesio A, Jazayeri M, Romo R, Salzman CD, Shadlen MN, Fusi S (2020) Low-dimensional dynamics for working memory and time encoding. Proc Natl Acad Sci USA.

Desrochers TM, Chatham CH, Badre D (2015) The necessity of rostrolateral prefrontal cortex for higher-level sequential behavior. Neuron 87:1357–1368.

Esmailpour H, Raman R, Vogels R (2023) Inferior temporal cortex leads prefrontal cortex in response to a violation of a learned sequence. Cereb Cortex 33:3124–3141.

Genovesio A, Tsujimoto S, Wise SP (2006) Neuronal Activity Related to Elapsed Time in Prefrontal Cortex. Journal of Neurophysiology 95:3281–3285.

Grohn J, Schüffelgen U, Neubert F-X, Bongioanni A, Verhagen L, Sallet J, Kolling N, Rushworth MFS (2020) Multiple systems in macaques for tracking prediction errors and other types of surprise. PLoS Biol 18:e3000899.

Jean-Baptiste Poline MB (2002) Region of interest analysis using an SPM toolbox.

Kim HF, Hikosaka O (2013) Distinct basal ganglia circuits controlling behaviors guided by flexible and stable values. Neuron 79:1001–1010.

Leaver AM, Lare JV, Zielinski B, Halpern AR, Rauschecker JP (2009) Brain Activation during Anticipation of Sound Sequences. J Neurosci 29:2477–2485.

Leite FP, Tsao D, Vanduffel W, Fize D, Sasaki Y, Wald LL, Dale AM, Kwong KK, Orban G a, Rosen BR, Tootell RBH, Mandeville JB (2002) Repeated fMRI using iron oxide contrast agent in awake, behaving macaques at 3 Tesla. NeuroImage 16:283–294.

815 McLaren DG, Kosmatka KJ, Oakes TR, Kroenke CD, Kohama SG, Matochik JA, Ingram DK,
816 Johnson SC (2009) A population-average MRI-based atlas collection of the rhesus
817 macaque. NeuroImage 45:52–59.

818 Meyer T, Qi X-L, Stanford TR, Constantinidis C (2011) Stimulus Selectivity in Dorsal and
819 Ventral Prefrontal Cortex after Training in Working Memory Tasks. J Neurosci 31:6266–
820 6276.

821 Miyashita Y, Higuchi SI, Sakai K, Masui N (1991) Generation of fractal patterns for probing the
822 visual memory. Neuroscience Research 12:307–311.

823 Niki H, Watanabe M (1979) Prefrontal and cingulate unit activity during timing behavior in the
824 monkey. Brain Res 171:213–224.

825 Onoe H, Komori M, Onoe K, Takechi H, Tsukada H, Watanabe Y (2001) Cortical Networks
826 Recruited for Time Perception: A Monkey Positron Emission Tomography (PET) Study.
827 NeuroImage 13:37–45.

828 Petrides M, Pandya DN (1999) Dorsolateral prefrontal cortex: comparative cytoarchitectonic
829 analysis in the human and the macaque brain and corticocortical connection patterns. Eur
830 J Neurosci 11:1011–1036.

831 Rainer G, Rao SC, Miller EK (1999) Prospective Coding for Objects in Primate Prefrontal
832 Cortex. J Neurosci 19:5493–5505.

833 Rapan L, Froudist-Walsh S, Niu M, Xu T, Zhao L, Funck T, Wang X-J, Amunts K, Palomero-
834 Gallagher N (2023) Cytoarchitectonic, receptor distribution and functional connectivity

835 analyses of the macaque frontal lobe Badre D, Baker CI, Thiebaut de Schotten M, eds.
836 eLife 12:e82850.

837 Sallet J, Mars RB, Noonan MP, Neubert F-X, Jbabdi S, O'Reilly JX, Filippini N, Thomas AG,
838 Rushworth MF (2013) The organization of dorsal frontal cortex in humans and
839 macaques. J Neurosci 33:12255–12274.

840 Sirmpilatze N, Klink PC (2020) RheMAP: Non-linear warps between common rhesus macaque
841 brain templates. Available at: https://zenodo.org/records/3668510 [Accessed July 10,
842 2024].

843 Stern CE, Sherman SJ, Kirchhoff BA, Hasselmo ME (2001) Medial temporal and prefrontal
844 contributions to working memory tasks with novel and familiar stimuli. Hippocampus
845 11:337–346.

846 Suda Y, Tada M, Matsuo T, Kawasaki K, Saigusa T, Ishida M, Mitsui T, Kumano H, Kirihara K,
847 Suzuki T, Matsumoto K, Hasegawa I, Kasai K, Uka T (2022) Prediction-Related Frontal-
848 Temporal Network for Omission Mismatch Activity in the Macaque Monkey. Front
849 Psychiatry 13:557954.

850 Tang H, Bartolo R, Averbeck BB (2021) Reward-related choices determine information timing
851 and flow across macaque lateral prefrontal cortex. Nat Commun 12:894.

852 Uhrig L, Dehaene S, Jarraya B (2014) A Hierarchy of Responses to Auditory Regularities in the
853 Macaque Brain. J Neurosci 34:1127–1132.

854 Vanduffel W, Farivar R (2014) Functional MRI of Awake Behaving Macaques Using Standard
855 Equipment. In: Advanced Brain Neuroimaging Topics in Health and Disease
856 (Papageorgiou TD, Christopoulos GI, Smirnakis SM, eds), pp Ch. 6. Rijeka: IntechOpen.
857 Available at: https://doi.org/10.5772/58281 [Accessed March 9, 2023].

858 Vergnieux V, Vogels R (2020) Statistical Learning Signals for Complex Visual Images in
859 Macaque Early Visual Cortex. Front Neurosci 14:789.

860 Walker AE (1940) A cytoarchitectural study of the prefrontal area of the macaque monkey.
861 Journal of Comparative Neurology 73:59–86.

862 Wang L, Uhrig L, Jarraya B, Dehaene S (2015) Representation of numerical and sequential
863 patterns in macaque and human brains. Current Biology 25:1966–1974.

864 Xu R, Bichot NP, Takahashi A, Desimone R (2022) The cortical connectome of primate lateral
865 prefrontal cortex. Neuron 110:312-327.e7.

866 Yamagata T, Nakayama Y, Tanji J, Hoshi E (2012) Distinct information representation and
867 processing for goal-directed behavior in the dorsolateral and ventrolateral prefrontal
868 cortex and the dorsal premotor cortex. J Neurosci 32:12934–12949.

869 Yusif Rodriguez N, McKim TH, Basu D, Ahuja A, Desrochers TM (2023) Monkey Dorsolateral
870 Prefrontal Cortex Represents Abstract Visual Sequences during a No-Report Task. J
871 Neurosci 43:2741–2755.

872

873